INTEGRATED FLUID-THERMAL-STRUCTURAL ANALYSIS USING ADAPTIVE UNSTRUCTURED MESHES

ICAS-90-2.9.3

Pramote Dechaumphai*
NASA Langley Research Center
Hampton, Virginia
USA

Abstract

An integrated fluid-thermal-structural analysis approach using adaptive unstructured meshes is presented. The approach combines the finite element method and an adaptive remeshing technique to solve: (1) the Navier-Stokes equations for high-speed compressible flow, (2) the energy equation for the thermal response of the structure, and (3) the quasi-static equilibrium equations for the structural response. The analysis solution procedure and the adaptive unstructured remeshing technique are described. The effectiveness of the approach is evaluated with three application studies. The flow analysis of Mach 8 shock-shock interference on a three-inch-diameter cylinder is used as the first application to demonstrate the capability of the adaptive remeshing technique to capture the physics features of a complex high-speed flow. The thermal analysis of a plate subjected to highly localized surface heating is used as the second application to demonstrate the efficiency of the approach for reducing the analysis solution error and the problem size. The applicability of the approach for the thermal and structural analyses of the structure is evaluated in the third application of a 0.25-inch-diameter convectively cooled leading edge subjected to intense aerodynamic heating. The adaptive unstructured remeshing procedure and finite element solution algorithms combine to yield increased accuracy and efficiency over standard structured meshes.

Nomenclature

A	coolant passage area, Eq. (5), or finite element area, Eq. (10)
[A*]	Jacobian matrix, Eq. (8)
[B]	viscous flux matrix, Eq. (11)
c	specific heat, Eq. (4), or material elastic constants, Eq. (18)
e	error
E, F	x and y flux components, respectively
H	load vector, Eq. (3)
h	convective heat transfer coefficient, Eq. (5), or element spacing parameter, Eq. (22)
[I]	identity matrix
[K]	stiffness matrix
k	thermal conductivity
l, m	components of unit normal vector
$\dot{m}$	coolant mass flow rate
[M]	mass matrix
[N]	element interpolation or weighting function
$\bar{n}$	unit normal vector
P	coolant passage perimeter
p	pressure
q	heat flux
{R}	load vector
s	edge length of finite element
T	temperature
T_o	reference temperature for zero stress
t	time, Eq. (1), or plate thickness, Eq. (30)
U	conservation variable
u, v	flow velocity components, Eq. (2), or displacement components, Eq. (19)
x, y	coordinate directions
X,Y	principal coordinate directions
Δt	time step
ΔU	$U^{n+1}-U^n$
α	temperature gradient parameter
β	thermal expansion parameter
ε	flow total energy, Eq. (2), or strain components, Eq. (18)
λ	eigenvalues
ϕ	key parameter for remeshing, Eq. (20)
ρ	density
$\sigma_x, \sigma_y, \tau_{xy}$	fluid stress components, Eq. (2), or solid stress components, Eq. (7)

Subscripts

c	coolant
F	fluid
L	left element
R	right element
T	thermal
S	structural
1	element internal flux
2	flux across element boundary

Superscripts

I	inviscid
V	viscous
T	transpose
i,j	summation indices
n	time step index, $t_n = n\Delta t$

Introduction

Design of lightweight structures and thermal protection systems for hypersonic vehicles depends on accurate prediction of aerothermal loads, structural temperatures and their gradients, and structural deformations and stresses. Adaptive unstructured remeshing techniques combined with the finite element method have been shown to significantly improve the efficiency and accuracy of the flow analysis. These benefits should accrue for both the thermal and structural analyses of structures. In addition, a universal

*Aerospace Technologist, Aerothermal Loads Branch, Structural Mechanics Division, Member AIAA

remeshing procedure is needed for the development of an integrated fluid-thermal-structural analysis capability.

Research is currently underway at NASA Langley Research Center to develop an integrated analysis approach for accurately predicting fluid, thermal, structural behavior and their interactions. The approach uses the finite element method to solve: (1) the Navier-Stokes equations for the aerodynamic flow field and the aerothermal loads; (2) the structural energy equation for heat transfer and temperature distribution; and (3) the structural equilibrium equations for deformation and stresses. The capability of the approach was demonstrated in Ref. [1] for an undisturbed Mach 6 flow over a three-inch-diameter stainless steel cylinder for which experimental data[2] were available for comparison. The flow field is characterized by the bow shock that stands-off the cylinder and the thin boundary layer at the cylinder surface. Sharp gradients in the flow variables occur in these regions and closely spaced elements were generated manually to model these flow features. The flow solution compares well with the experimental data demonstrating the effectiveness of the finite element method used.

For a more complex problem, where a priori knowledge of the flow physics does not exist, an appropriate finite element mesh may not be constructed or even be designed easily. An adaptive mesh generation technique is required not only to construct and adapt the mesh automatically to represent the flow field but also to minimize the number of unknowns and the analysis computational time. Thus the current focus on the improvement of the integrated analysis approach is to develop efficient adaptive unstructured mesh generation techniques for each analysis discipline considered including their interface requirements.

Adaptive mesh generation techniques may be classified into two major categories: (1) refinement/derefinement, and (2) remeshing. The first category, the adaptive refinement/derefinement technique, can be further classified into three subcategories: (a) the h method, (b) the p method, and (c) the r method. In the h method, the elements in the initial mesh are refined into smaller elements or derefined into larger elements[3]. The p method maintains the geometry of the elements of the initial mesh but increases (or decreases) the order of the polynomial used for the element interpolation function[4]. The r method keeps the number of elements and their connectivities the same but relocates the nodes[5]. These methods help increase the analysis solution accuracy but each has limitations. Even though nodes could be added or removed by the h method, the orientation of the original and new elements may not change. Orientation of element sides along principal flow gradients increases solution accuracy and reduces the number of elements[6]. Even though the r method can move the nodes for better alignment, the method may generate highly distorted elements if the number of elements is fixed. The p method may alleviate these restrictions because of the flexibility in selecting the order of polynomials on the element sides. However, the use of such higher order polynomials in combination with the hierarchical concept leads to complexities in the formulation of finite element equations and implementation in computer programs.

The above considerations led to the development of the second adaptive mesh category, the remeshing technique[7]. The technique generates an entirely new mesh based on the solution obtained from the earlier mesh. The technique combined with the finite element method has been applied successfully to several compressible flow problems with complex flow behavior[8-10]. The purpose of this paper is to extend the adaptive remeshing technique to both the thermal and structural analyses of structures. An error estimation technique applicable for adaptive unstructured meshes will be described. An adaptive remeshing technique will be evaluated to assess its effectiveness for integrated fluid-thermal-structural analysis. The equations for the aerodynamic flow, structural heat transfer, and structural response will be given. The analysis solution algorithms for solving these equations will be described. The basic concepts of the adaptive remeshing technique will then be explained. Selection of indicators used for construction of new meshes for the three analysis disciplines will be discussed. Finally the adaptive remeshing technique will be evaluated for: (1) the fluid analysis of Mach 8 shock-shock interference on a three-inch-diameter cylinder where experimental data are available, (2) the thermal analysis of a plate subjected to highly localized surface heating, and (3) the thermal-structural analysis of a 0.25-inch-diameter convectively cooled leading edge subjected to intense aerodynamic heating simulating a Mach 16 flight condition. The requirements for the mesh continuity along the fluid/structure interface and between thermal and structural analyses for direct interdisciplinary data transfer will also be discussed.

Fluid-Thermal-Structural Analysis Procedure

Mathematical Formulation

The equations for the aerodynamic flow, the structure heat transfer, and the structural response in two dimensions are briefly described herein.

Aerodynamic Flow. The equations for a laminar compressible flow are governed by the conservation of mass, momentum, and energy. These equations are written in conservation form as

$$\frac{\partial}{\partial t}\{U_F\} + \frac{\partial}{\partial x}\{E_F\} + \frac{\partial}{\partial y}\{F_F\} = 0 \qquad (1)$$

where the subscript F denotes the fluid analysis. The conservation variables vector, $\{U_F\}$, and the flux vectors in the x and y directions, $\{E_F\}$ and $\{F_F\}$, are given by

$$\{U_F\}^T = [\rho \quad \rho u \quad \rho v \quad \rho \varepsilon]$$

$$\{E_F\}^T = [E_F]^I + [E_F]^V$$
$$= [\rho u \quad \rho u^2+p \quad \rho uv \quad \rho u\varepsilon+pu]$$
$$- [0 \quad \sigma_x \quad \tau_{xy} \quad u\sigma_x+v\tau_{xy}-q_x]$$

$$\{F_F\}^T = [F_F]^I + [F_F]^V$$
$$= [\rho v \quad \rho uv \quad \rho v^2+p \quad \rho v\varepsilon+pv]$$
$$- [0 \quad \tau_{xy} \quad \sigma_y \quad u\tau_{xy}+v\sigma_y-q_y] \qquad (2)$$

Superscripts I and V represent the inviscid and viscous flux vector components, respectively. The pressure p is related to the total energy assuming a calorically perfect gas (constant ratio of specific heats). The stresses σ_x,

σ_y, and τ_{xy} are related to the velocity gradients by Stokes's law. The heat fluxes q_x and q_y are related to the temperature gradients by Fourier's law. The temperature-dependent viscosity is computed from Sutherland's law and the thermal conductivity is computed assuming a constant Prandtl number of 0.72.

Structural Heat Transfer. The thermal response of the structure is obtained from the energy equation which is written in conservation form as

$$\frac{\partial}{\partial t}(U_T) + \frac{\partial}{\partial x}(E_T) + \frac{\partial}{\partial y}(F_T) = H_T \qquad (3)$$

where the subscript T denotes the thermal analysis. For transient heat conduction, the conservation variable, U_T, and the heat flux components, E_T and F_T, are

$$\begin{aligned} dU_T &= \rho_s c_s dT_s \\ E_T &= q_x = -k_s\, \partial T_s/\partial x \\ F_T &= q_y = -k_s\, \partial T_s/\partial y \end{aligned} \qquad (4)$$

and H_T is the heat source. The structural heat flux components q_x and q_y are related to the temperature gradients by Fourier's law.

For a structure with internal convective cooling, the energy equation for the coolant flow in the local x-direction (flow direction) based on assumed uniform cross-sectional or bulk temperature[1], T_c, can also be written in the conservation form of Eq. (3) where

$$\begin{aligned} dU_T &= \rho_c c_c dT_c \\ E_T &= \dot{m} c_c T_c/A_c - k_c\, \partial T_c/\partial x \\ F_T &= 0 \\ H_T &= hP\,(T_s - T_c) \end{aligned} \qquad (5)$$

The flux E_T consists of the energy transport by convection (1st term) and conduction (2nd term), and the flux H_T represents the heat transfer between the structure and the coolant.

Structural Response. The structural response is obtained from the quasi-static equilibrium equations assuming that the inertia effects are negligible. These equations are written in conservation form as

$$\frac{\partial}{\partial x}\{E_s\} + \frac{\partial}{\partial y}\{F_s\} = 0 \qquad (6)$$

The flux vector components, $\{E_S\}$ and $\{F_S\}$, are

$$\begin{aligned} \{E_s\}^T &= [\ \sigma_x \quad \tau_{xy}\ ] \\ \{F_s\}^T &= [\ \tau_{xy} \quad \sigma_y\ ] \end{aligned} \qquad (7)$$

where the stress components, σ_x, σ_y, and τ_{xy} are related to the displacement gradients and the temperature by the generalized Hooke's law.

Analysis Solution Algorithms

An implicit/explicit upwind cell-centered algorithm[8] is used to solve the Navier-Stokes equations given by Eqs. (1)-(2)[11]. A flux-based Taylor-Galerkin finite element algorithm[10,12] is used to solve the thermal and structural equations given by Eqs. (3)-(7). For brevity, only essential features of the algorithms are highlighted herein.

Upwind Fluid Algorithm. The basic concept behind the upwind cell-centered algorithm is to assume a constant distribution of the conservation variables over an element. The flux across element interfaces is determined by Roe's averaging procedure[13]. The average inviscid flux $\{\bar{E}\}^I$ (the "overbar" denotes an average quantity normal to the element interface between the left element, L, and the right element, R) is given by

$$\{\bar{E}\}^I = \frac{1}{2}\left[\{\bar{E}_L\}^I + \{\bar{E}_R\}^I + [\,|A^*|\,](\{U_L\} - \{U_R\})\right] \qquad (8)$$

where $[|A^*|]$ denotes a matrix whose entries are the absolute values of those in the Jacobian matrix $[A^*]$. The Jacobian matrix $[A^*]$ is associated with the element flow velocity components and the local speed of sound. Details of the Jacobian matrix $[A^*]$ are given in Ref. [13].

In the computation of viscous flux components such as the heat flux in the x-direction ($q_x = -k_F\, \partial T/\partial x$), the element temperature gradient is computed from

$$\frac{\partial T(x,y)}{\partial x} = [N(x,y)]\left\{\frac{\partial T}{\partial x}\right\} \qquad (9)$$

where $[N(x,y)]$ is a row matrix of finite element interpolation functions. The vector on the right hand side of the equation contains the nodal temperature gradients, determined at node K, by

$$\frac{\partial T}{\partial x}\Big|_K = \frac{1}{M_K}\left(\int_s \bar{n}\, T\, N_K\, ds - \int_A T\, \frac{\partial N_K}{\partial x}\, dA\right) \qquad (10)$$

where $\bar{n}$ is the unit normal vector along the element interface s and M_K is the lumped mass at node K.

Increments in time of the element conservation variables, $\Delta U = U^{n+1} - U^n$, are determined from

$$\left[[I] + \frac{\Delta t}{A}\sum_s \left([\,|A^*|\,]\frac{s}{2} - [B]\right)\right]\{\Delta U\} = -\frac{\Delta t}{A}\sum_s s\,[\{\bar{E}\}^I + \{\bar{E}\}^V] \qquad (11)$$

The matrix [B], which is associated with the viscous fluxes is given in Refs. [8,11], accelerates the solution convergence in the viscous dominated regions. This fluid algorithm provides first order of accuracy (O(h)) in the inviscid flow dominated region, but the order of accuracy is close to 1.5 ($O(h^{1.5})$) in the viscous flow dominated region[11].

Flux-Based Taylor-Galerkin Algorithm. The basic concept of the flux-based Taylor-Galerkin algorithm is to express the element flux components E and F in the form

$$\begin{aligned} E(x,y,t) &= [N(x,y)]\{E(t)\} \\ F(x,y,t) &= [N(x,y)]\{F(t)\} \end{aligned} \qquad (12)$$

where {E}, and {F} are vectors of the element nodal flux quantities.

For the thermal analysis, the final finite element equations are in the form

$$[M]\{\Delta U_T\}^{n+1} = \{R_T\}_1^n + \{R_T\}_2^n \qquad (13)$$

where at time step n+1, $\Delta U^{n+1} = U^{n+1} - U^n$. The mass matrix, [M], is given by

$$[M] = \int_A \{N\}[N]\, dA \qquad (14)$$

The two vectors on the right hand side of Eq. (13) are associated with the fluxes within the element (subscript 1) and across the element boundary (subscript 2). These vectors are defined by

$$\{R_T\}_1^n = \Delta t \left(\int_A \{\frac{\partial N}{\partial x}\}[N]\, dA \{E_T\}^n + \int_A \{\frac{\partial N}{\partial y}\}[N]\, dA \{F_T\}^n \right) \qquad (15)$$

$$\{R_T\}_2^n = -\Delta t \int_S \{N\}[N]\, ds \left(l\{E_T\}^n + m\{F_T\}^n\right) = -\Delta t \int_S \{N\}[N]\, ds \{q\}^n \qquad (16)$$

The vectors $\{E_T\}$ and $\{F_T\}$ contain nodal heat fluxes which depend on the nodal temperature gradients. The element nodal temperature gradients $\partial T/\partial x$ and $\partial T/\partial y$, and all the finite element matrices (Eqs. (13)-(16)) can be evaluated in closed form (i.e., numerical integration is not required) for any type of finite element including the 4-node quadrilateral and the 8-node hexahedral elements.

For the structural analysis, the final finite element equations are in the same form as the thermal equation, Eq. (13), but without the transient term,

$$\{R_S\}_1 + \{R_S\}_2 = 0 \qquad (17)$$

where these vectors are identical to those in Eqs. (15)-(16) except that the subscript T is replaced by the subscript s everywhere. The element nodal flux vectors $\{E_S\}$ and $\{F_S\}$ (similar to $\{E_T\}$ and $\{F_T\}$ in Eq. (15)) now consist of the stress components σ_x, σ_y, and τ_{xy}. By using the thermal stress-strain constitutive relations,

$$\sigma_i = c_{ij}\varepsilon_j + \beta_i (T - T_o) \qquad i,j = 1,2,3 \qquad (18)$$

and the strain-displacement relations, these nodal stress components associated with the $\{R_S\}_1$ vector can be written in terms of the nodal displacement components. Further algebraic manipulation of the finite element equation, Eq. (17), results in the standard form of

$$[K]\{U_S\} = \{R_S\}_2 + \{R_T\} \qquad (19)$$

where $\{U_S\}$ consists of the unknowns of the nodal displacement components, [K] is the element stiffness matrix, and $\{R_T\}$ is the thermal load vector. These matrices are evaluated in closed form and the details are given in Ref. [12].

Adaptive Remeshing Procedure

Remeshing Concept

The basic idea of adaptive remeshing is to construct a completely new mesh based on the solution obtained from the previous mesh. The new mesh will consist of clustered elements in regions with large changes in solution gradients and few elements in the regions where the gradient changes are small. Element orientations are aligned with principal directions to provide the most accurate solution with a minimum number of elements. As an example, the shorter element side is in the direction normal to the shock line or through the boundary layer thickness to model large solution gradients. Based on these ideas, the adaptive remeshing technique consists of two steps: (1) the determination of the new element sizes and their orientations, and (2) the construction of the new mesh.

In the determination of the element size and orientation, the solid mechanics concept of determining the principal stresses and their directions from a given state of stress at a point is employed. For example in the thermal analysis, small and clustered elements are needed in regions of large change in the temperature gradients. The temperature is thus considered as a key parameter to indicate where elements need to be clustered. At a typical node in the old mesh, the second derivative[7,11] of the key parameter, ϕ, for remeshing with respect to the global coordinates x and y are first computed,

$$\begin{bmatrix} \frac{\partial^2\phi}{\partial x^2} & \frac{\partial^2\phi}{\partial x \partial y} \\ \frac{\partial^2\phi}{\partial x \partial y} & \frac{\partial^2\phi}{\partial y^2} \end{bmatrix} \qquad (20)$$

Then the eigenvalues, λ, which represent the principal quantities in the principal directions X and Y where the cross derivatives vanish are determined,

$$\lambda_1 = \left| \frac{\partial^2\phi}{\partial X^2} \right| \quad \text{and} \quad \lambda_2 = \left| \frac{\partial^2\phi}{\partial Y^2} \right| \qquad (21)$$

These eigenvalues are the remeshing indicators and are used to determine the element (nodal) spacings h_1 and h_2 in the two principal directions using the condition that

$$h_1^2 \lambda_1 = h_2^2 \lambda_2 = \text{constant} \qquad (22)$$

which result from distributing the finite element interpolation error equally, a condition for an optimal mesh[14]. This process is performed for all the nodes in the old mesh leading to the final condition[7] of

$$h_1^2 \lambda_1 = h_2^2 \lambda_2 = \text{constant} = h_{min}^2 \lambda_{max} \qquad (23)$$

Using this condition and specifying the required minimum element spacing, h_{min}, the new element spacings based on the solution of the old mesh are obtained and the new mesh is constructed.

The approach used for mesh construction is based on an advancing front technique[7]. Nodes are first placed along the domain boundary. Spacings between these nodes are dictated by the element spacing parameter h obtained earlier. At this instance, the front consists of a sequence of straight line segments which connect consecutive boundary nodes, i.e., the domain boundary. Elements adjacent to the domain boundary are then constructed. The sizes and orientations of these elements are guided by the computed element spacing parameter h, the principal directions, and the allowable element aspect ratio. As new elements are constructed from the domain boundary, the front is updated and represented by the new element sides. As the mesh construction goes on, the front changes its shape and propagates toward the domain interior. The generation process is terminated when the domain is filled completely with elements and the front vanishes.

Based on the condition shown in Eq. (23), the element size is generated according to the given minimum element spacing h_{min}. Specifying too small a spacing h_{min} can result in a model with a large number of elements which may be impractical. On the other hand, specifying too large a spacing h_{min} may result in poor solution accuracy, or an excessive number of analysis and remeshing cycles to achieve the required solution accuracy. These factors must be considered prior to generating a new mesh. Note that, because the technique generates an entirely new mesh with different nodal locations from the old mesh, interpolation of the solution from the old to the new mesh is necessary. The interpolated nodal quantities are used as the initial conditions for the new mesh to increase the analysis solution convergence.

Fluid-Thermal-Structural Remeshing Parameters

The adaptive remeshing technique described requires a selection of proper key parameters (ϕ in Eq. (20)) for remeshing so that generated elements are properly sized, oriented, and clustered. Selection of the key parameters depends on the analysis discipline and its applications. In general, dependent variables are usually selected as the key parameters for remeshing. In the inviscid flow field of high-speed compressible flow problems, the fluid density is normally selected as the key parameter[7,10] because density exhibits high gradients across shock and flow expansion waves. In the viscous dominated flow regions, such as the boundary layer, other key parameters may be more appropriate. Key parameters of heating rate and skin friction may be used for more accurate analysis prediction of the aerothermal loads[11].

For thermal problems, the temperature is selected as the key parameter so that the mesh generated can represent steep temperature gradients. For structural problems, stress is an appropriate choice for the key parameter so that regions with high stress concentration will be represented. However, the key parameter representing the stress should be a scalar quantity such as the Von Mises stress defined by,

$$\sigma_{\text{Von Mises}} = \frac{1}{\sqrt{2}} \sqrt{(\sigma_x - \sigma_y)^2 + \sigma_x^2 + \sigma_y^2 + 6\tau_{xy}^2} \qquad (24)$$

Note that the key parameter selected for remeshing may vary with applications. For problems that require accurate deformations rather than the stresses, an absolute displacement quantity may be preferred as the key parameter. The selection of these key parameters for remeshing in the three different analysis disciplines will be discussed in detail in the application section. Note that, for coupled interdisciplinary analysis, the key parameters for remeshing will have to be combined to produce an optimum mesh for each discipline and their interaction.

Error Indicator

In the structural analysis formulation described previously, the unknown displacements are assumed to be continuous across elements. Once the nodal displacements are determined from Eq. (19), the element stress components (σ_x, σ_y, τ_{xy}) are then computed using Eq. (18). For triangular elements, the computed stress components are constant over elements and thus discontinuous across element boundaries. These constant element stresses which deviate from the actual (exact) smooth stress distribution may be used to estimate the solution error. This idea was proposed by Zienkiewicz and Zhu[15] who estimated solution error by computing the difference between the predicted discontinuous element stresses and a smoothed stress distribution obtained by smoothing the element stresses. The smoothed stress distribution may not be the exact stress distribution, but in general, approximates the exact stress distribution better than the discontinuous element stresses. The effectiveness of this approach has been demonstrated for several structural problems[15] such as a beam bending problem, a plane stress problem, etc. In this paper, the approach is adapted to the thermal analysis and its effectiveness is evaluated using a heat transfer problem with a known exact solution.

For the thermal analysis, the smooth flux distribution in the x-direction, q_x^*, is assumed to vary over an element in the form,

$$q_x^*(x,y) = [N(x,y)] \{ \bar{q}_x^* \} \qquad (25)$$

where $\{ \bar{q}_x^* \}$ is the vector of the unknown nodal values of the smooth flux. These unknown nodal values are determined by applying the method of weighted residuals to the difference between the smooth flux distribution, q_x^*, and the predicted discontinuous element flux, $\hat{q}_x$,

$$\int_A [N]^T (q_x^* - \hat{q}_x) \, dA = 0 \qquad (26)$$

Substituting Eq. (25) into Eq. (26) yields,

$$[M] \{\bar{q}_x^*\} = \int_A [N]^T \, dA \, \hat{q}_x \qquad (27)$$

where [M] is the mass matrix defined in Eq. (14). Equation (27) is written for each element and assembled to form a global system of equations. If the mass matrix [M] is lumped, the system of equations can be solved explicitly for the nodal fluxes. The nodal values for the smooth flux in the y-direction are determined in the same fashion.

The L^2 norm of the estimated error in heat fluxes over an element is then defined as,

$$\| e \| = [\int_A ((q_x^* - \hat{q}_x)^2 + (q_y^* - \hat{q}_y)^2) \, dA]^{1/2} \qquad (28)$$

and the L^2 norm of the global error is,

$$\| e \|_{global} = [\sum_{element} \| e \|^2]^{1/2} \qquad (29)$$

The normalized L^2 norm of the global error is defined by,

$$\eta_{flux} = \frac{\| e \|_{global}}{\| e \|_{global} + \| q^* \|} \times 100\% \qquad (30)$$

where

$$\| q^* \| = [\sum_{element} \int_A ((q_x^*)^2 + (q_y^*)^2) \, dA]^{1/2} \qquad (31)$$

The computed L^2 norms are used as a posteriori measure of the solution accuracy for different finite element models. For a heat transfer problem with a known exact solution, both q_x^* and q_y^* in Eqs. (28) are replaced by the exact heat flux components. Highly accurate numerical integration is used to compute the L^2 norm of the exact error over an element and for the entire computational domain using Eqs. (28)-(29), respectively. The effectiveness of this error estimation technique is evaluated for both uniformly refined meshes and adaptive unstructured meshes in the second application.

Evaluation of Integrated Analysis and Adaptive Remeshing Procedures

Three applications are presented to assess the adaptive unstructured remeshing procedures for fluid-thermal-structural analysis. The fluid analysis of Mach 8 shock-shock interference on a three-inch-diameter cylinder is used as the first application to illustrate the successful implementation of the adaptive remeshing technique for complex flow and the interface requirements with the thermal and structural analyses of the structure. The capability of the adaptive remeshing technique for reducing the solution error is demonstrated in the second application for the thermal analysis of a plate subjected to highly localized surface heating. The applicability of the remeshing technique for integrated thermal and structural problems is demonstrated in the third application for a 0.25-inch-diameter convectively cooled leading edge subjected to intense aerodynamic heating. Remeshing parameters for separate thermal and mechanical stress predictions, as well as for combined thermal/mechanical stress analysis, are identified.

Mach 8 Shock-Shock Interference On a Cylinder

Leading edges of hypersonic vehicles that experience intense stagnation point pressures and heating rates are a significant challenge to the designer. For engine leading edges, such as the cowl shown in Fig. 1, intense aerothermal loads occur when the cowl bow shock is intersected by an oblique shock resulting in a supersonic jet that impinges on the leading edge surface. The experimental configuration (lower left of Fig. 1), which simulates the vehicle forebody and cowl leading edge, was used to define the aerothermal loads[2,16]. The experimental configuration is rotated 180° relative to the vehicle. The schlieren photograph shows the supersonic jet interference pattern impinging on the surface of the cylinder. The interference pattern produces intense local amplification of the pressure and heat transfer rate in the vicinity of the jet impingement.

To predict the aerothermal loads and to capture the complex flow phenomena, the flow over the three-inch-diameter cylinder with the computational domain shown by the rectangular enclosure in the experimental configuration (lower left of Fig. 1) is analyzed[17]. The inflow conditions above and below the oblique shock are: (1) Mach 8.03 flow at an angle of attack of zero degrees and static temperature of 200 °R, and (2) Mach 5.25 flow at an angle of attack of 12.5 degrees and a static temperature of 430 °R. A total of three subsequent adaptive unstructured meshes are used in the analysis. These meshes consists of triangles in the inviscid region and quadrilateral elements in the boundary layer. Quadrilateral elements are used in the boundary layer to capture steep temperature gradients for accurate aerodynamic heating rate prediction. Details of the flow mathematical model and the three adaptive meshes are given in Ref. [17]. The flow analysis starts from using the first mesh to predict the flow solution. Based on this flow solution and the use of the fluid density as the key parameter for remeshing, the second adaptive mesh is created. The flow solution obtained from the first mesh is then interpolated and used as the initial condition for the second mesh. The same procedure is repeated to construct the third mesh and to obtain the corresponding flow solution. Details of the flow solutions corresponding to these three adaptive meshes are also given in Ref. [17].

The third adaptive mesh and the corresponding flow solution in the form of temperature contours in the interaction region are highlighted in Fig. 2. The figure shows elements are concentrated along the incident shock, the bow shock, and the supersonic jet to capture the steep flow gradients. The fluid temperature increases sharply across the bow shock from a relatively low temperature (200 °R and 430 °R) to approximately 2,700 °R. In the thin boundary layer, the temperature drops sharply to the cylinder surface temperature of 530 °R resulting in high aerodynamic heating rate.

The analytically predicted surface pressure distribution and the experimentally measured pressures[2] are normalized by the undisturbed stagnation pressure and are compared in Fig. 3. Good agreement between the analytical and experimental results are obtained for

the pressure distribution, the peak pressure and its locations. The analytically predicted surface heating rate normalized by the undisturbed stagnation heating rate is compared with the experimentally measured heating rate in Fig. 4. Even though the predicted and experimental heating rate distributions agree well, the peak predicted heating rate amplification, q/q_0, is only about 60% of that measured from the experiment. The lower predicted heating rate may be attributed to several sources including the finite element mesh, the analysis algorithm, and the mathematical model. On the other hand, the higher experimental heating rate may be attributed to the free stream turbulence which is not taken into account in the analysis.

To generate an integrated fluid-thermal-structural finite element model, the use of common nodes along the fluid/structure interface is preferred[18] as highlighted in Fig. 5. This approach not only permits direct data transfer between the different analysis disciplines but also provides consistency for the analysis formulation. As an example of a coupled fluid/thermal problem, the interface nodal temperatures can be obtained by solving the coupled energy equation of the flow and the structure[1] with the requirements that at the interface: (1) the temperatures of the fluid and the structure are identical, and (2) the heat flux is continuous.

For some problems, the requirement of common fluid/structure interface nodes to preserve the mesh continuity may result in an excessive number of nodes in one of the discipline models. For example, a high stress concentration may occur near the fluid/structure interface which may require a large number of the structural nodes even though the flow near that region is simple. Several adaptive meshing techniques are feasible for the thermal-structural analysis of the structure as indicated in Fig. 5 which include the mesh refinement/derefinement technique and the remeshing technique developed for the flow problems. Before selecting one of these techniques, their effectiveness for thermal and structural problems must be evaluated. An initial evaluation of the adaptive remeshing technique for both the thermal and structural analyses is performed in the next two applications.

Plate with Surface Heating

To demonstrate the benefits of using adaptive unstructured meshes and to evaluate the error estimation technique described, the thermal analysis of a unit square plate with thickness t subjected to an applied surface heating distribution[19] is performed. The plate temperature distribution, which is a solution to the Poisson's equation with boundary conditions of zero temperature along the four edges, is shown in Fig. 6. The applied surface heating distribution is given by,

$$\frac{q}{kt} = 2y(1-y)\left[\tan^{-1}\beta - \frac{\alpha(1-2x)}{\sqrt{2}\,(1+\beta^2)} + \frac{\alpha^2\beta x(1-x)}{2(1+\beta^2)^2}\right] + 2x(1-x)\left[\tan^{-1}\beta - \frac{\alpha(1-2y)}{\sqrt{2}\,(1+\beta^2)} + \frac{\alpha^2\beta y(1-y)}{2(1+\beta^2)^2}\right] \quad (32)$$

where

$$\beta = \alpha\left(\frac{x+y}{\sqrt{2}} - 0.8\right) \quad (33)$$

The exact solution for the temperature distribution is,

$$T = x(1-x)y(1-y)\tan^{-1}\beta \quad (34)$$

The temperature contours for the exact solution with α = 100 are shown in Fig. 6. The figure shows steep temperature gradients along a line perpendicular to the s-direction at s = 0.8.

Both the temperature and the applied surface heating distributions along the plate diagonal in the s-direction are shown in Fig. 7. The figure shows the steep gradients and the rapid change in surface heating distribution in a narrow domain around s = 0.8. The shape of the surface heating distribution is similar to that generated by complex flow such as shown in the first application (see Fig. 4). The steep gradients in the surface heating requires a refined mesh to accurately prescribe its magnitude and distribution to obtain accurate temperature predictions.

Both uniformly refined meshes and adaptive unstructured meshes are used in the analysis. For the uniformly refined meshes, a total of seven finite element models (not shown) are employed. The first model consists of 200 triangles and 121 nodes with 11 nodes equally spaced in each x and y direction. The seventh model consists of 9800 triangles and 5041 nodes with 71 nodes equally spaced in each x and y direction. The three adaptive unstructured meshes used in the analysis are shown in Fig. 8. The first adaptive mesh is constructed from the temperature solution obtained from the third uniform refinement model (31X31 nodes) using temperature as the key parameter for remeshing. The thermal analysis is then performed on this first adaptive mesh to predict the temperature solution. The same procedure is repeated to construct the second and the third adaptive meshes and to predict their corresponding temperature solutions.

Because the exact temperature solution is known, the exact error in the predicted temperature distributions obtained from the uniformly refined meshes and the adaptive unstructured meshes can be computed. The L^2 norm of the exact global error for a predicted temperature is defined by,

$$\| e \|_{temp} = \left[\sum_{element} \int_A (T_{exact} - T_{predicted})^2 \, dA \right]^{1/2} \quad (35)$$

where T_{exact} is the exact temperature distribution given in Eq. (34) and $T_{predicted}$ is the finite element predicted temperature distribution. The normalized L^2 norm of the global error for the predicted temperature is defined by,

$$\eta_{temp} = \frac{\| e \|_{temp}}{\left[\sum_{element} \int_A T_{exact}^2 \, dA \right]^{1/2}} \times 100\ \% \quad (36)$$

The normalized L^2 norm of the global errors in the predicted temperatures from these finite element models are shown in Fig. 9. The figure shows that the errors on the adaptive meshes are reduced at a faster rate than for the uniform refinement. Solutions on the adaptive meshes converge at a faster rate since the smaller elements are clustered in the high temperature gradient regions.

This heat transfer problem is also used to evaluate the effectiveness of the error estimation technique described by Eqs. (25)-(31). For the three adaptive meshes, the smoothed flux distributions are computed

from the constant element flux components using Eq. (27). The L^2 norm of the estimated error in the heat fluxes for these meshes are then computed from Eqs. (28)-(29). The normalized L^2 norm of the estimated global errors in the heat fluxes (Eq. (30)) are plotted as a function of the number of nodes as shown in Fig. 10. Because the exact temperature solution is known, the exact heat fluxes can be determined and the L^2 norm of the exact error in the heat fluxes can be computed. The normalized L^2 norm of the exact global error in the heat fluxes for the three adaptive meshes are also shown in Fig. 10. The figure shows good agreement between the estimated and exact errors for all three meshes with a maximum difference of the normalized L^2 less than 3%. Hence for general problems where the exact solutions are not available, the estimated error may be used to ensure that the analysis solution errors are reduced with subsequent adaptive meshes. The applicability of this error estimation technique to a more complex problem is demonstrated in the next application.

Convectively Cooled Leading Edge

A 0.25-inch-diameter convectively cooled leading edge subjected to intense aerodynamic heating is used to evaluate the adaptive remeshing technique for both the thermal and structural analyses, and to identify requirements for the remeshing parameters for thermal stress problems. The example problem represents a hypersonic vehicle operating at Mach 16 which causes the vehicle nose bow shock to intersect with the cowl leading edge bow shock. The intersection produces the type IV supersonic jet interference pattern similar to that described in the first application. Because of the smaller leading edge diameter and the higher Mach number conditions, the heating rate is very intense with a peak of nearly 30,000 Btu/ft^2-sec (see Ref. [1]).

The leading edge geometry and boundary conditions are shown schematically in Fig. 11. The outer surface is subjected to the aerodynamic heating and emits radiant energy to space. The inner surface is convectively cooled by the direct impingement of a sonic hydrogen jet stream with an inlet temperature of 50 °R. The 1350 quadrilateral element mesh shown in Fig. 12(a) is typical of a structured mesh. The mesh has been used previously[1] for predicting transient thermal-structural response of the leading edge as the vehicle nose bow shock sweeps across the cowl during the vehicle acceleration. The mesh is graded in the radial direction but is uniform in the circumferential direction. The leading edge material is assumed to be copper because of its high thermal conductivity[1]. The predicted steady-state leading edge temperature contours are shown in Fig. 12(b). The peak temperature of 766 °R is at the jet impingement location where the heating rate is a maximum. Based on the error estimation technique described earlier, the normalized L^2 norm of the estimated global error in the heat fluxes (Eq. (30)) for this finite element model is approximately 9%.

The same adaptive remeshing procedure described in the first two applications is applied for the thermal analysis of the leading edge. Two adaptive unstructured meshes are constructed as shown in Fig. 13. The thermal analysis is performed and the temperature solutions for these two meshes are obtained. Using the error estimation technique, the normalized L^2 norm of the estimated global errors in the heat fluxes for these two models are 11% and 6%, respectively. These estimated errors indicate that the second adaptive mesh (Fig. 13(b)) provides better solution accuracy and requires only about a quarter of the number of unknowns compared to the nonadaptive mesh (Fig. 12(a)).

To evaluate the effectiveness of the adaptive remeshing technique to represent both the thermal and mechanical stress fields, structural boundary constraints at the upper and lower leading edge sections are introduced. The inner surface nodes at the constraint are fixed ($u = v = 0$, see Fig. 14(a)) to simulate the constraints caused by the internal fins that support the leading edge from the inner primary structure. To highlight the remeshing capability for generating clustered elements to capture both the thermal and mechanical stresses, the rest of the nodes on both sections are constrained differently. These nodes are free to move on the upper section, but are constrained in the horizontal direction on the lower section. In addition to the thermal loads, the leading edge is also subjected to mechanical loads from: (1) the aerodynamic pressure which has a distribution similar to that shown in Fig. 3 but with a peak pressure of 1,000 psia, and (2) the uniform internal coolant pressure of 1,000 psia.

The final adaptive unstructured thermal mesh shown in Fig. 13(b) is used as the initial mesh for the structural analysis. The same analysis procedure is applied by first obtaining the structural analysis solution and then remeshing. In the remeshing process, nodal temperatures of the new mesh are interpolated from the nodal temperatures of the thermal mesh shown in Fig. 13(b). For thermal stress problems, high stresses normally occur in regions of high temperature gradients. High stress concentrations may also occur at corners or supports even though the temperature is uniform. Thus, to represent both the thermal stress and the stress concentration, key parameters for remeshing based on the temperature and the Von Mises stress are used simultaneously. Each key parameter identifies an element size for equally distribution of the finite element interpolation error (see Eq. (23)), however, the minimum element size is always selected. A new adaptive mesh generated by using these two remeshing parameters is shown in Fig. 14(a). Elements are clustered near the jet impingement location for modeling high thermal stresses from the high temperature gradients, and at the region near the upper support where the mechanical stress concentration occurs. The corresponding structural response, based on a linear elastic behavior assumption, is shown by the circumferential stress contours superimposed on the deformed leading edge in Fig. 14(b). The figure shows that a peak circumferential compressive stress of 25 ksi occurs at the jet impingement location and a high stress concentration occurs near the singular point at the upper support.

Superposition of the solutions from different load cases is a popular technique in the structural analysis, hence the effect of adaptive unstructured remeshing on superpositioning is investigated. Since the thermal mesh is probably adequate for the thermal stress analysis, the adaptive remeshing technique for the structural analysis is further evaluated for the case in which the thermal load is not present. The leading edge is subjected only to the mechanical load which consists of the external aerodynamic pressure and the internal coolant pressure. The Von Mises stress is used as the remeshing parameter and the adaptive mesh generated is shown in

Fig. 15(a). Similar to the previous case, clustered elements are in the region near the upper support where the stress concentration occurs. The corresponding predicted structural response of the circumferential stress contours is shown in Fig. 15(b). The predicted circumferential compressive stress of 5 ksi at the jet impingement location is much lower than the stress that occurred for the case with the thermal load. Obviously, superposition of the solutions for separate mechanical and thermal stress analyses would require interpolation of the solutions which would result in decreased solution accuracy. Hence, the adaptive remeshing and analysis should be used for the combined load cases.

For coupled fluid-thermal-structural analysis, both the thermal and structural response of the leading edge can affect the flow field. The flow field has to be updated to include the effects of: (1) the change of the leading edge surface temperature, and (2) the leading edge deformation. To satisfy the first item, common nodes are needed along the fluid/structure interface to provide the continuity of the temperature and heat fluxes. For the second item, the leading edge may deform into or away from the initial flow field mesh and updating the flow computational domain is necessary. The new flow field may govern regions previously occupied by the leading edge where the flow information does not exist. These are some of the future issues which will be encountered and have to be clarified prior to applying the adaptive remeshing technique to coupled interdisciplinary problems. However, the adaptive unstructured remeshing procedure and the key parameters for remeshing presented herein demonstrate the viability of the approach for interdisciplinary analyses.

Concluding Remarks

An adaptive unstructured remeshing technique was evaluated for integrated fluid-thermal-structural analysis. The technique generates an entirely new mesh based on the solution obtained from a previous mesh. The new mesh consists of clustered elements in the regions with high solution gradients and few elements in the regions where the gradients are small. The capability of the remeshing technique was demonstrated for fluid, thermal, and structural analyses. The analysis formulations used for the three disciplines were presented. The basic idea behind the remeshing technique was described and the remeshing indicators and requirements were identified.

Three applications were presented to assess the effectiveness of the remeshing technique. The fluid analysis of Mach 8 shock-shock interference on a three-inch-diameter cylinder was presented as the first application to demonstrate the benefit of the remeshing technique for complex flow. Fluid density was used as the key parameter for remeshing. The thermal analysis of a plate subjected to surface heating with a known exact solution was used as the second application to demonstrate that the adaptive unstructured remeshing technique reduces the analysis solution error and increases the computational efficiency relative to structured meshes. The application also demonstrated the effectiveness of an error estimation technique, which was further applied to a more complex problem in the third application to ensure that the analysis solution error reduces with the subsequent adaptive meshes. In this third application, the applicability of the remeshing technique to thermal stress problems was demonstrated with a 0.25-inch-diameter convectively cooled leading edge subjected to intense aerodynamic heating. Temperature was selected as the remeshing parameter in the thermal analysis so that clustered elements are generated in regions of high temperature gradients. The remeshing technique provides less solution error with significant reduction in the number of unknowns as compared to a structured mesh. For the structural analysis of the leading edge subjected to both thermal and pressure loads, remeshing parameters of the temperature and the Von Mises stress were used simultaneously to provide an optimum mesh with clustered elements in regions of high thermal and mechanical stresses as well as regions with a stress concentration. The mesh is for the combined thermal and mechanical load cases to avoid the superposition of the solutions from each separate load case which would decrease the solution accuracy.

The results from the applications have demonstrated the viability of the adaptive unstructured remeshing technique combined with the finite element methods to provide efficient accurate solutions to complex flow-thermal-structural behavior.

References

1. Dechaumphai, P., Thornton, E. A. and Wieting, A. R., "Flow-Thermal-Structural Study of Aerodynamically Heated Leading Edges," AIAA Journal of Spacecraft and Rockets, Vol. 26, No. 4, July 1989, pp. 201-209.
2. Wieting, A. R. and Holden, M. S., "Experimental Shock-Wave Interference Heating on a Cylinder at Mach 6 and 8," AIAA Journal, Vol. 27, No. 11, November 1989, pp. 1557-1565.
3. Ramakrishnan, R., Bey, K. S. and Thornton, E. A., "Adaptive Quadrilateral and Triangular Finite Element Scheme for Compressible Flows," AIAA Journal, Vol. 28, No. 1, January 1990, pp. 51-59.
4. Thornton, E. A. and Dechaumphai, P., "Adaptive Refinement for Effective Finite Element Thermal and Structural Analyses," International Conference on Accuracy Estimates and Adaptive Refinements in Finite Element Computations, Lisbon, Portugal, Vol. 2, 1984, pp. 65-74.
5. Lohner, R., Morgan, K. and Zienkiewicz, O. C., "Adaptive Grid Refinement for Compressible Euler and Navier-Stokes Equations," International Conference on Accuracy Estimates and Adaptive Refinements in Finite Element Computations, Lisbon, Portugal, Vol. 2, 1984, pp. 189-202.
6. Morgan, K., Peraire, J., Thareja, R. R. and Stewart, J. R., "An Adaptive Finite Element Scheme for Euler and Navier-Stokes Equations," AIAA Paper No. 87-1172, June 1987.
7. Peraire, J., Vahdati, M., Morgan, K. and Zienkiewicz, O. C., "Adaptive Remeshing for Compressible Flow Computations," Journal of Computational Physics, Vol. 72, 1987, pp. 449-466
8. Thareja, R. R., Stewart, J. R., Hassan, O., Morgan, K. and Peraire, J., "A Point Implicit Unstructured Grid Solver for the Euler and Navier Stokes Equations," International Journal for Numerical Methods in Fluids, Vol. 9, 1989, pp. 405-425.
9. Dechaumphai, P. and Wieting, A. R., "Coupled Fluid-Thermal-Structural Analysis for

Aerodynamically Heated Structures," Finite Element Analysis in Fluids, Edited by Chung, T. J. and Karr, G. R., The University of Alabama in Huntsville Press, April 1989, pp. 165-171.
10. Dechaumphai, P., Wieting, A. R. and Pandey, A. K., "Fluid-Thermal-Structural Interaction of Aerodynamically Heated Leading Edges," AIAA Paper No. 89-1227-CP, April 1989.
11. Vemaganti, G. R., "An Adaptive Remeshing Finite Element Method for High Speed Compressible Flows Using Quadrilateral and Triangular Elements," Ph.D. Dissertation, Old Dominion University, May 1989.
12. Pandey, A. K., Dechaumphai, P. and Wieting, A. R., "Thermal-Structural Finite Element Analysis Using Linear Flux Formulation," AIAA Paper No. 89-1224-CP, April 1989.
13. Gnoffo, P. A., "Application of Program LAURA to Three-Dimensional AOTV Flowfields," AIAA Paper No. 86-0565, January 1986.
14. Oden, J. T. and Carey, G. F., Finite Elements: Mathematical Aspects, Prentice-Hall, Englewood Cliffs, 1981.
15. Zienkiewicz, O. C. and Zhu, J. Z., "A Simple Error Estimator and Adaptive Procedure for Practical Engineering Analysis," International Journal for Numerical Methods in Engineering, Vol. 24, 1987, pp. 337-357.
16. Holden, M. S., Wieting, A. R., Moselle, J. R. and Glass, C., "Study of Aerothermal Loads Generated in Region of Shock/Shock Interaction in Hypersonic Flow," AIAA Paper No. 88-0477, January 1988.
17. Dechaumphai, P., "Evaluation of an Adaptive Unstructured Remeshing Technique for Integrated Fluid-Thermal-Structural Analysis," AIAA Paper No. 90-0556, January 1990.
18. Thornton, E. A. and Dechaumphai, P., "Coupled Flow, Thermal, and Structural Analyses of Aerodynamically Heated Panels," AIAA Journal of Aircraft, Vol. 25, No. 11, November 1988, pp. 1052-1059.
19. Rachowicz, W., Oden, J. T. and Demkowicz, L., "Toward a Universal h-p Adaptive Finite Element Strategy, Part 3," Texas Institute for Computational Mechanics, University of Texas at Austin, TICOM Report 89-03, 1989, p.56.

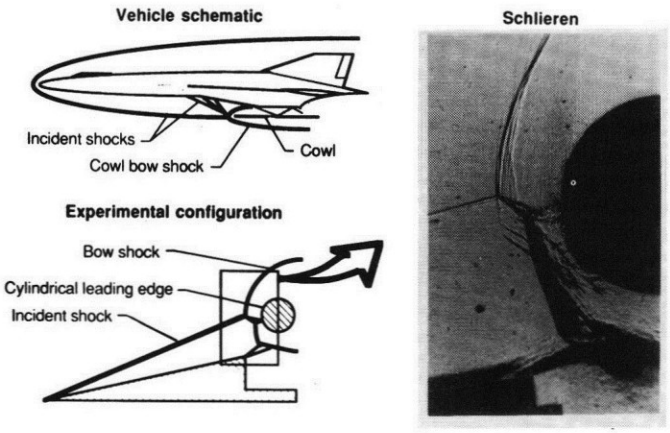

Fig. 1 Vehicle schematic, experimental configuration, and schlieren of type IV shock-shock interference.

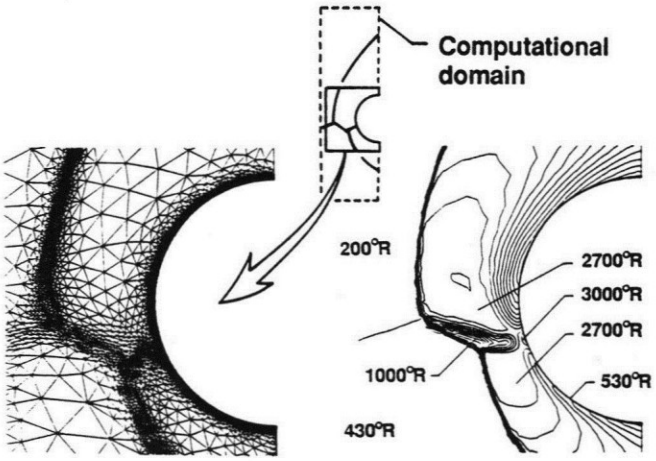

Fig. 2 Details of the finite element mesh and fluid temperature contours in the interaction region for Mach 8 shock-shock interference on a three-inch-diameter cylinder.

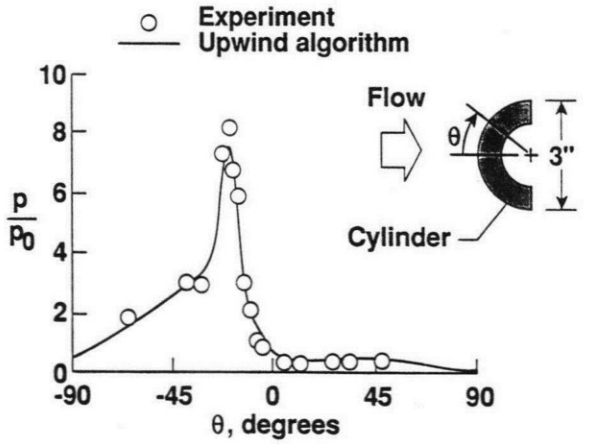

Fig. 3 Comparison of surface pressure distributions on a three-inch-diameter cylinder subjected to Mach 8 shock-shock interference.

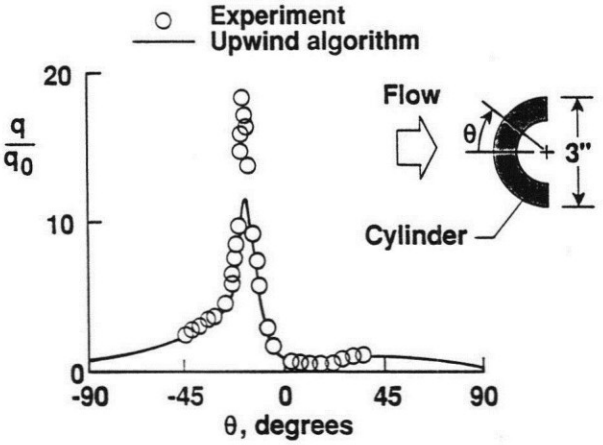

Fig. 4 Comparison of surface heating rate distributions on a three-inch-diameter cylinder subjected to Mach 8 shock-shock interference.

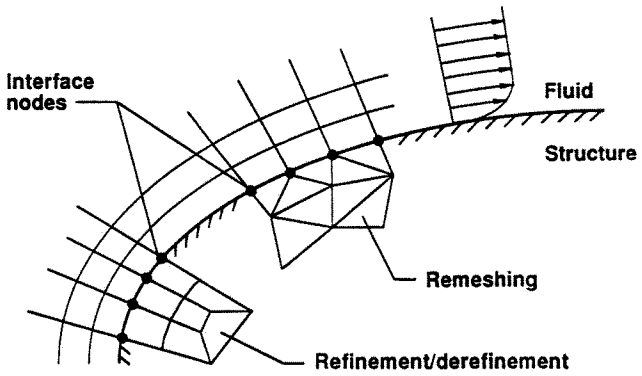

Fig. 5 Integrated fluid-thermal-structural mesh concept and adaptive meshing options for thermal-structural analysis of the structure.

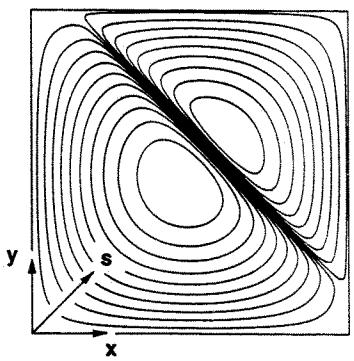

$$\frac{\partial^2 T}{\partial x^2} + \frac{\partial^2 T}{\partial y^2} = -\frac{q}{kt}$$

for $0 < x < 1$; $0 < y < 1$

with $T = 0$ along edges

$\frac{q}{kt}$ and $T(x,y)$ are given in Eqs. (30)-(31).

Fig. 6 Governing differential equation, boundary conditions, and temperature solution for a unit square plate subjected to a nonuniform surface heating.

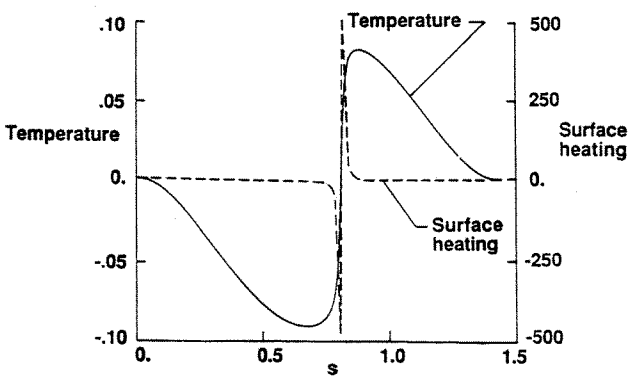

Fig. 7 Plate temperature and surface heating distributions along a diagonal direction of the plate.

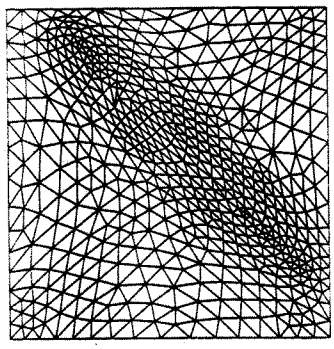

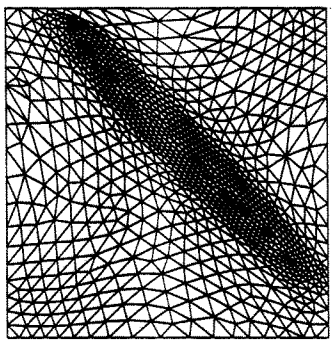

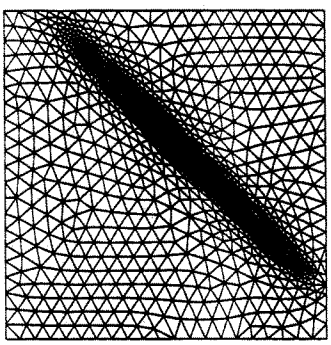

First adaptive mesh

1058 Elements
563 Nodes

Second adaptive mesh

1655 Elements
866 Nodes

Third adaptive mesh

2014 Elements
1051 Nodes

Fig. 8 Sequence of adaptive finite element meshes for a plate subjected to a nonuniform surface heating.

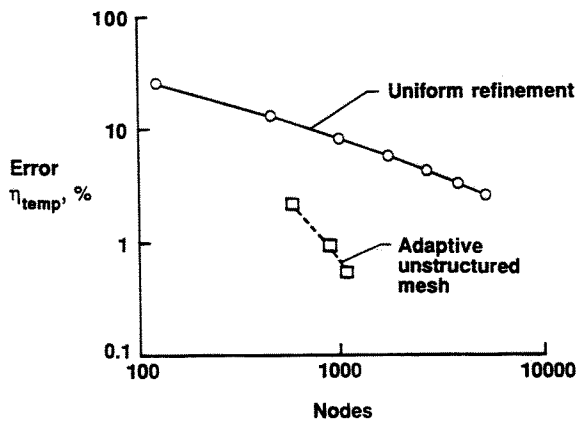

Fig. 9 Comparison of the normalized L^2 norm of the exact global error in the plate temperature solutions (Eq. (36)) for the uniformly refined meshes and the adaptive unstructured meshes.

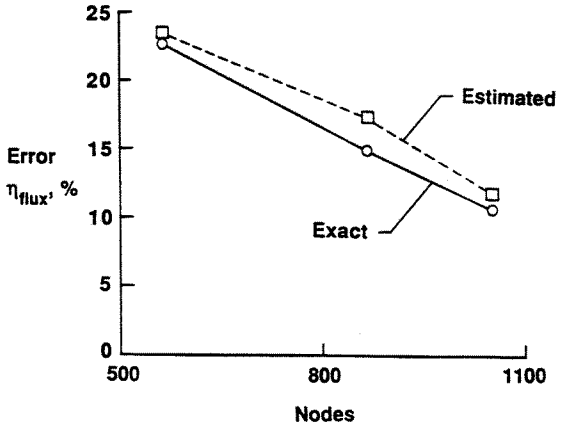

Fig. 10 Comparison of the normalized L^2 norm of the estimated and exact errors in the plate heat fluxes (Eq. (30)) using the three adaptive unstructured meshes.

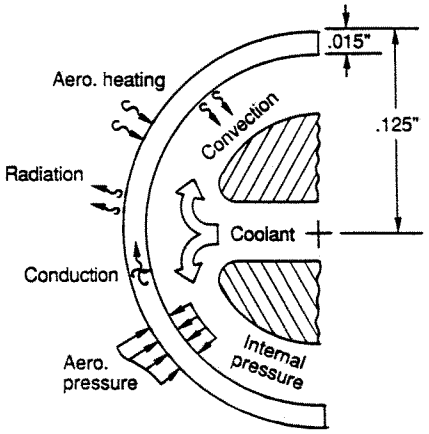

Fig. 11 A schematic thermal-structural analysis model of 0.25-inch-diameter leading edge with boundary conditions.

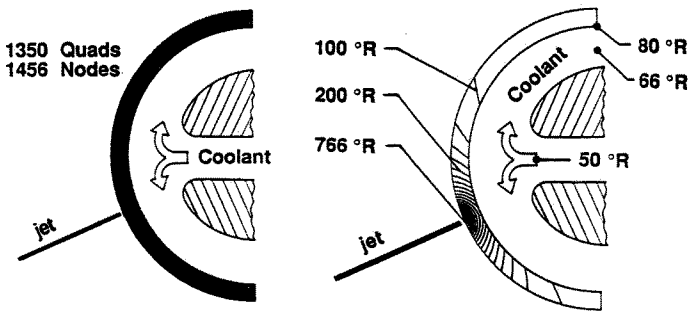

(a) Nonadaptive structured mesh (b) Temperature contours

Fig. 12 Nonadaptive finite element mesh and temperature contours for convectively cooled leading edge.

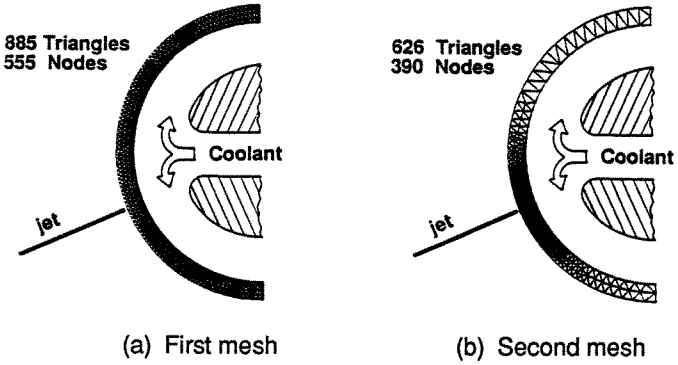

(a) First mesh (b) Second mesh

Fig. 13 Adaptive finite element mesh evolution for thermal analysis of convectively cooled leading edge.

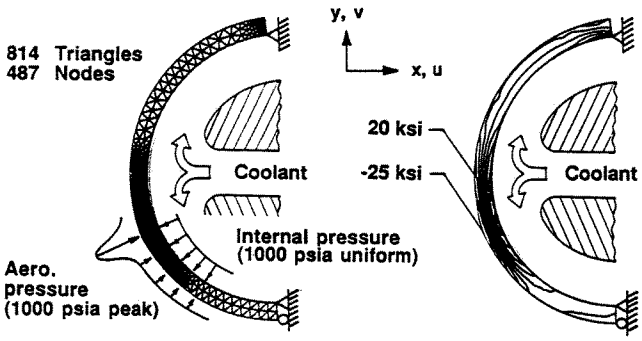

(a) Adaptive mesh (b) Circumferential stress

Fig. 14 Final adaptive mesh and circumferential stress for convectively cooled leading edge subjected to thermal and pressure loads.

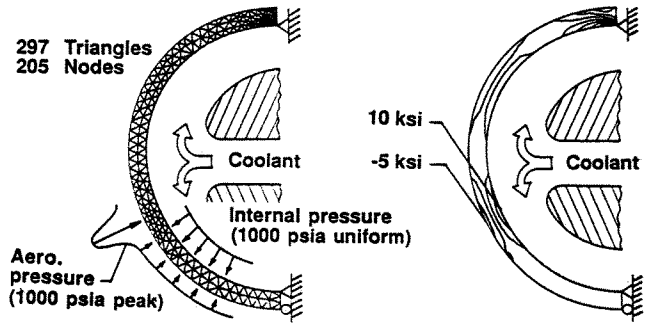

(a) Adaptive mesh (b) Circumferential stress

Fig. 15 Final adaptive mesh and circumferential stress for convectively cooled leading edge subjected to pressure load.